HIFAN 1727

HEAVY ION FUSION SCIENCE VIRTUAL NATIONAL LABORATORY 2nd QUARTER 2009 MILESTONE REPORT

Perform beam and target experiments with a new induction bunching module, extended FEPS plasma, and improved target diagnostic and positioning equipment on NDCX.

by

F.M. Bieniosek, A. Anders, J.J. Barnard, M.R. Dickinson, E. Gilson, W. Greenway, E. Henestroza, J.Y. Jung, T. Katayanagi, B.G. Logan, C.W. Lee, M. Leitner, S. Lidia, R. M. More, P. Ni, A. Pekedis, M. J. Regis, P.K. Roy, P. A. Seidl, W. Waldron

LBNL

Accelerator Fusion Research Division
Ernest Orlando Lawrence Berkeley National Laboratory
University of California
Berkeley, California 94720

MARCH 2009

This work was supported by the Director, Office of Science, Office of Fusion Energy Sciences, of the U.S. Department of Energy under Contract No. DE-AC02-05CH11231.

HEAVY ION FUSION SCIENCE VIRTUAL NATIONAL LABORATORY

2nd QUARTER 2009
MILESTONE REPORT

Perform beam and target experiments with a new induction bunching module, extended FEPS plasma, and improved target diagnostic and positioning equipment on NDCX.

F.M. Bieniosek, A. Anders, J.J. Barnard, M.R. Dickinson, E. Gilson, W. Greenway, E. Henestroza, J.Y. Jung, T. Katayanagi, B.G. Logan, C.W. Lee, M. Leitner, S. Lidia, R. M. More, P. Ni, A. Pekedis, M. J. Regis, P. K. Roy, P. A. Seidl, W. Waldron, for the HIFS-VNL

March 31, 2009

1. SUMMARY

This effort contains two main components: The new induction-bunching module is expected to deliver higher fluence in the bunched beam, and the new target positioner will enable a significantly enhanced target physics repetition rate.

The velocity ramp that bunches the K^+ beam in the neutralized drift compression section is established with a bipolar voltage ramp applied to an acceleration gap. An induction acceleration module creates this voltage waveform. The new bunching module (IBM) specially built for NDCX has approximately twice the capability (volt-seconds) as our original IBM. We reported on the beam line design for the best use of the bunching module in our FY08 Q2 report. Based on simulations and theoretical work, we chose to extend the drift compression section and use the additional volt-seconds to extend the pulse duration and keep the peak voltage swing (and velocity excursions) similar to the present module. Simulations showed that this approach, which extends the drift section, to be advantageous because it limits the chromatic aberrations in the beam spot on target. To this end, colleagues at PPPL have fabricated the meter-long extension to the ferro-electric plasma source and it was installed on the beam line with the new IBM in January 2009. Simulation results suggest a factor of two increase in energy deposition from the bunched beam.

In the first WDM target run (August – November 2008) the target handling setup required opening the vacuum system to manually replace the target after each shot (which destroys the target). Because of the requirement for careful alignment of each individual target, the target shot repetition rate was no greater than 1 shot per day. Initial results of this run are reported in our FY08 4th Quarter Milestone Report. Based on the valuable experience gained in the initial run, we have designed and installed an improved target alignment and positioning system with the capability to reposition targets remotely. This capability allows us to significantly increase our shot repetition rate, and to take greater advantage of the pinhole/cone arrangement we have developed to localize the beam at final focus. In addition we have improved the capability of the optical diagnostic systems, and we have installed a new beam current transformer downstream of the target to monitor beam current transmitted through the target during an experiment. These improvements will allow us to better exploit the inherent capability of the NDCX facility for high repetition rate and thus to provide more detailed experimental data to assess WDM physics models of target behavior.

This milestone has been met by demonstrating highly compressed beams with the new bunching module, which are neutralized in the longer drift compression section by the new ferro-electric plasma sources. The peak uncompressed beam intensity (≈600 kW/cm^2) is higher than in previous measurements, and the bunched beam current profiles are ≈2ns.

We have also demonstrated a large increase in the experimental data acquisition rate for target heating experiments. In the first test of the new remote-controlled target

positioning system, we completed three successful target physics shots in less than two hours. Further improvements are expected.

2. INTRODUCTION

The US heavy ion fusion science program is developing techniques for heating ion-beam-driven warm dense matter (WDM) targets [1-4]. Intense ion beams have several attractive features as a technique for generating WDM. These features include:
-Precise control of local beam energy deposition dE/dx, nearly uniform throughout a given volume, and not strongly affected by target temperature,
-Large sample sizes (about 1 micron thick by 1 mm diameter),
-The ability to heat any target material, for example, foams, powders, conductors, insulators, solid, gas, etc.

The WDM conditions are achieved by combined longitudinal and transverse space-charge neutralized drift compression of the ion beam to provide a hot spot on the target with a beam spot size of about 1 mm, and compressed pulse length about 2 ns. The experiments use a 0.3 MeV, 30-mA K^+ beam (below the Bragg peak) from the NDCX accelerator to heat foil targets such as Au, Al and Si. The NDCX beam contains an uncompressed pulse length up to 20 μs with a peak energy flux ≈600 kW/cm^2, and a compressed pulse of fluence ~10 mJ/cm^2.

A detailed description of the new experimental target chamber, targets, and target diagnostics was reported in the 3rd Quarter 2008 milestone report [1]. The WDM target diagnostics include a high-speed multi-channel optical pyrometer, optical streak camera, VISAR, and high-speed gated cameras [1,5]. The fast optical pyrometer is a unique and significant new diagnostic which provides valuable information on the temperature evolution of the heated target [6]. Initial target experiments in the new target chamber are described in the 4th Quarter 2008 Milestone Report. [5] In those experiments the beam heated 150-nm Au targets above 3000 K.

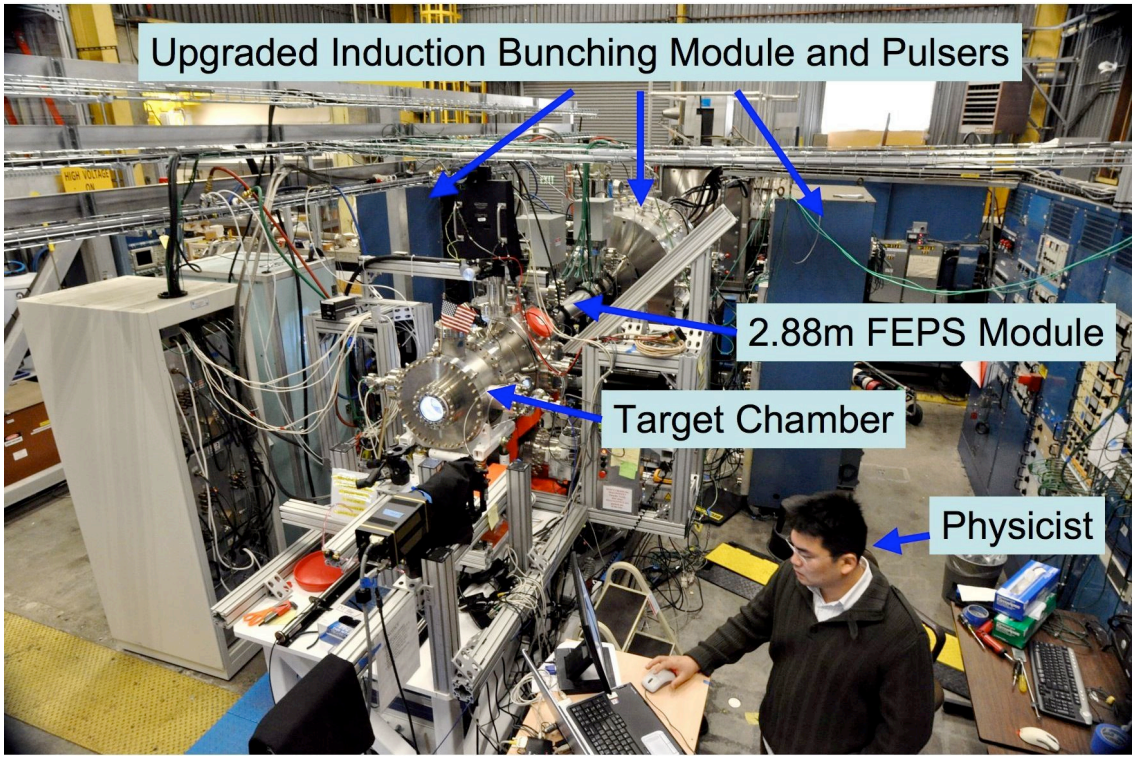

Fig. 1: Upgraded NDCX beamline and facility.

3. NDCX INDUCTION BUNCHING MODULE UPGRADE

A new induction bunching module (IBM) has been installed on the NDCX beamline (Fig. 1). This module holds 20 independently-driven 50%-Ni, 50%-Fe Astron cores that supply voltage to a 3cm long acceleration gap approximately 283 cm downstream from the ion source.

The IBM cores are driven by dedicated pulsed power circuits. An 18-kV, 27-nF charging circuit produces a 16-kV peak gap potential over a ~600-ns (full width) pulse in the IBM gap, as shown in Fig. 2. A capacitive voltage monitor in the gap region delivers a monitor signal with a calibration of 12 kV/V. The useful integrated volt-seconds in the main region of the waveform is 4.9 kV-μs, or 98 kV-μs for the entire module. Because the core losses are not sufficient to critically damp the circuit, there is some voltage reversal delivered to the gap following the main pulse. This ~0.6-kV-μs pulse represents approximately 12% of the main pulse volt-seconds and contributes to the final tuned waveform.

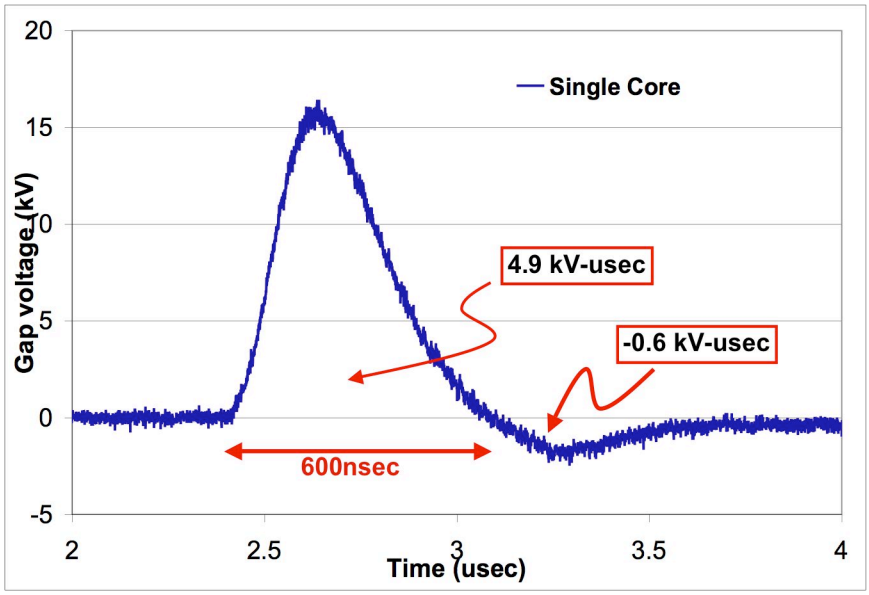

Fig. 2: Single core pulsed waveform voltage measured at the IBM gap.

The voltage waveform generated in the IBM produces the velocity chirp necessary to longitudinally compress the ion beam. The ideal waveform is an optimization for utilizing the increased number of IBM volt-seconds while maintaining the same absolute voltage swing. Doing so increases the total amount of beam charge that will evolve dynamically into a longitudinal current peak while holding constant the degree of chromatic defocusing in the compressed pulse which limits the compressed pulse intensity on target. The tuned waveform is presented in Fig. 3 with the ideal waveform superposed. The voltage difference is also shown and is limited to a range of 6kV over the 600ns useful working section of the waveform. This is to be compared with similar results from the previous IBM and tune, shown in Fig. 4. The previous IBM and tune also displayed a 6-kV difference range from the ideal, but over a much shorter duration (~220-ns) pulse. The larger number of independently-tunable induction cores (20) in the present IBM compared to the previous IBM (12 were used) allows for greater accuracy and finesse in fine tuning details.

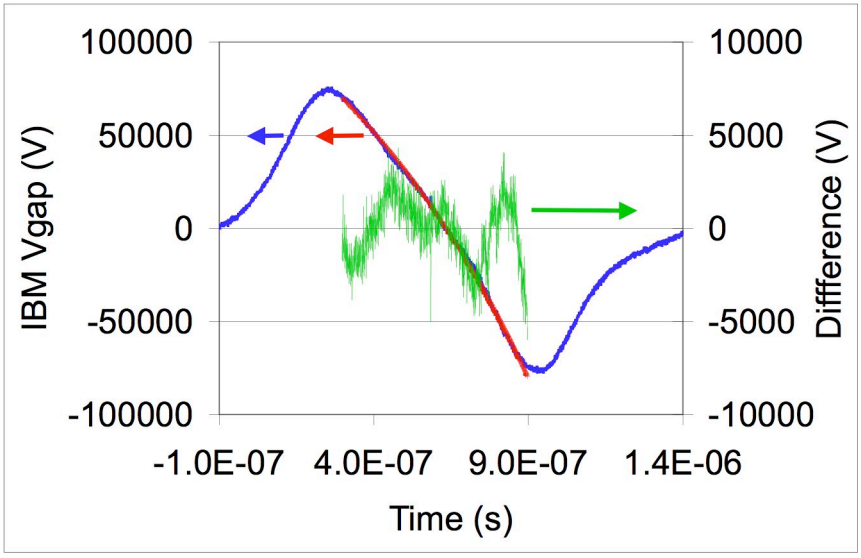

Fig. 3: Tuned IBM waveform (blue), Ideal waveform (red), and the difference (green).

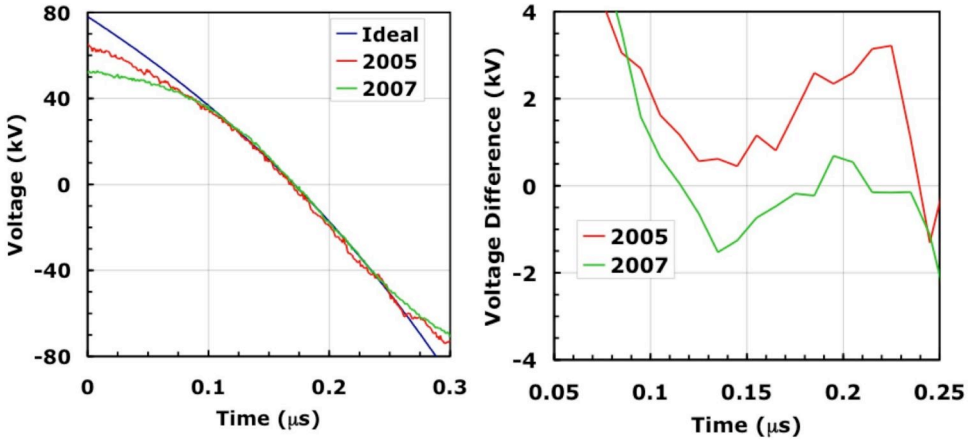

Fig. 4: (Left) Ideal and portions of the measured waveforms in the previous IBM; (right) Difference waveforms between measured and ideal.

An important measure of the efficiency of the IBM is how efficiently are the individual core waveforms utilized in composing the final, delay-tuned waveform from their sum. In the current hardware implementation, 10 of the IBM cores have a positive voltage polarity (similar to Fig. 2), while the other 10 cores have negative polarities. Practical issues such as fitting to a slightly nonlinear ideal waveform, asymmetrical single core waveforms and reversed-polarity components of single core waveforms require that some cancellation of impressed gap voltage occurs at various times during the full waveform. This has a detrimental effect to the overall system efficiency, but can be managed to a tolerable level while still achieving high quality waveforms.

If we define the net efficiency of the waveform tune as the product of the fraction of the full waveform volt-seconds in the ideal range (i.e. the 'working section') with the fraction of the total single-core volt-seconds (for 20 cores) in the full waveform range:

$$\eta_{net} = \frac{|Volt-seconds\ in\ ideal\ range|}{|Volt-seconds\ in\ full\ range|} \times \frac{|Volt-seconds\ in\ full\ range|}{|Volt-seconds\ in\ single\ core| \times N_{cores}}$$

= (28.1/55.2)*(55.2/(4.9*20)) = (0.51)*(0.56) = 0.29, or ~30%.

Note that we are evaluating the absolute value of the voltage amplitude for a bipolar waveform.

The new IBM has been utilized to create compressed beam pulses, which are then transported to the target chamber. The Fast Faraday Cup in the target chamber is used to measure the temporal profile of the ion beam after longitudinal compression, and in the presence of a high density ~10^{13} cm^{-3} background plasma. Initial beam measurements employing a non-optimized IBM tune readily yielded compressed pulses carrying ~2 A peak current with pulse durations ~2.4 ns (FWHM). An example is shown in Fig. 5. Improved tuning will increase the captured and compressed ion beam charge significantly.

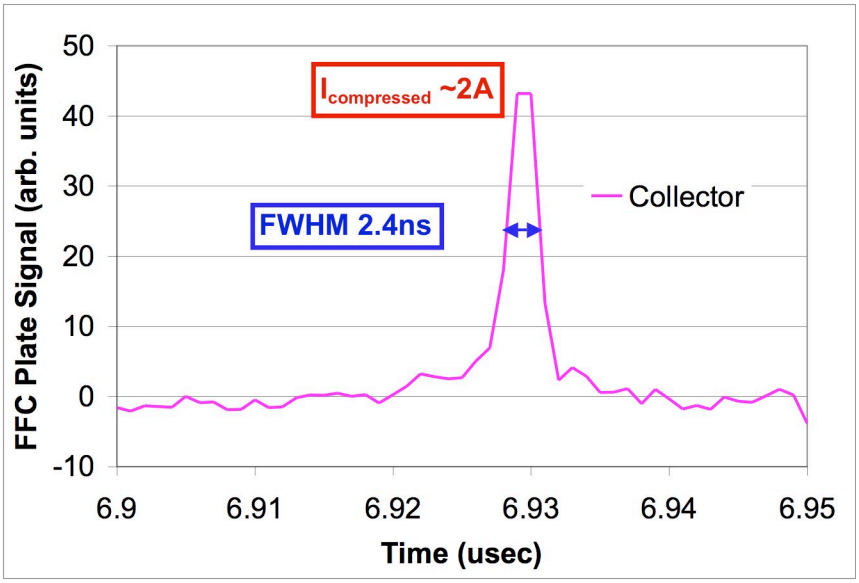

Fig. 5: Compressed pulse waveform measured in the target chamber.

4. BEAM TRANSPORT THROUGH LENGTHENED FEPS SECTION TO TARGET CHAMBER

The newly installed sections of the Ferro-Electric Plasma Source (FEPS) have been integrated with the previously installed sections, extending the overall neutralized drift length from 1.44 m to 2.88 m. A picture of the new FEPS module before installation is shown in Fig.6.

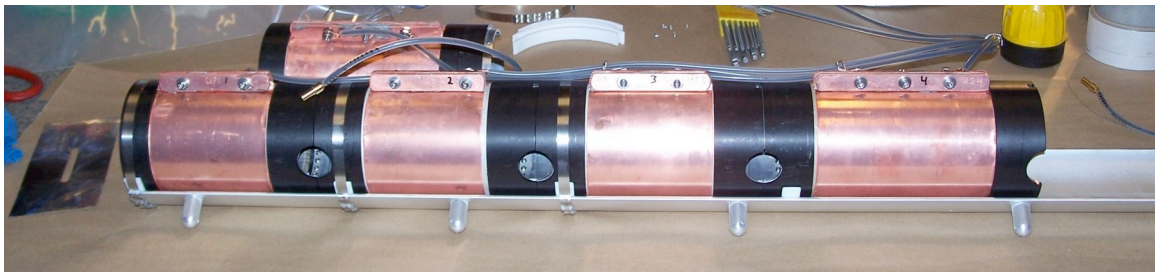

Fig. 6: New FEPS module prior to installation.

An initial round of tuning the matching solenoids upstream from the IBM has been performed. Fig. 7 shows the variation of the beam spot size (50% intensity radius) at the target plane as the peak field in the final solenoid (S4) is varied. For this beam energy (284 kV), a minimum spot size is seen for ≈1.7 T S4 peak field. For peak fields greater than 1.8 T the beam distribution is hollow, and the spot size is several times larger.

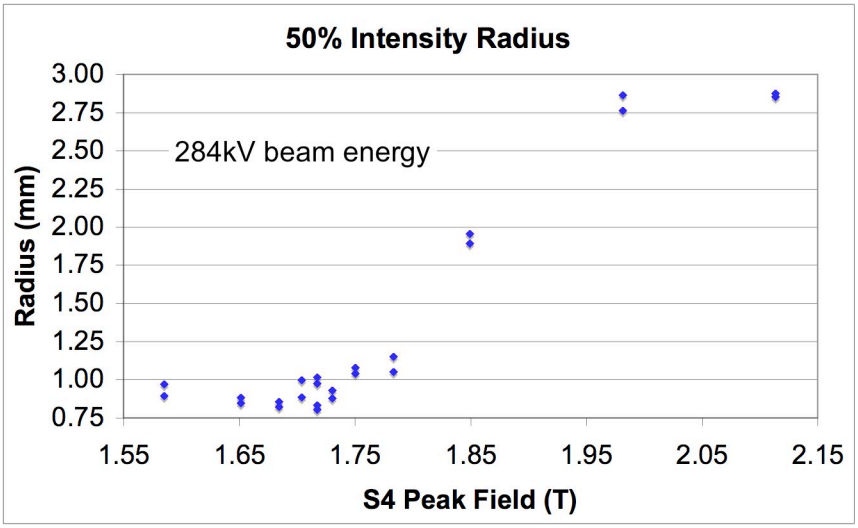

Fig. 7: Parametric scan of beam spot radius with final matching solenoid field.

The peak intensity has been measured at the target plane, and an initial parametric scan has been performed by varying first the peak solenoid field in S4 and then the beam energy itself (with energy dependent solenoid field scaling). The variation of peak intensity with solenoid field is shown in Fig. 8. The peak intensity is seen to correspond to the solenoid tune that produces the smallest beam spot size. The variation in peak and 50% beam intensity with beam energy is shown in Fig. 9. We see that at the lower energy range, the peak beam intensity can surpass 600 kW/cm^2.

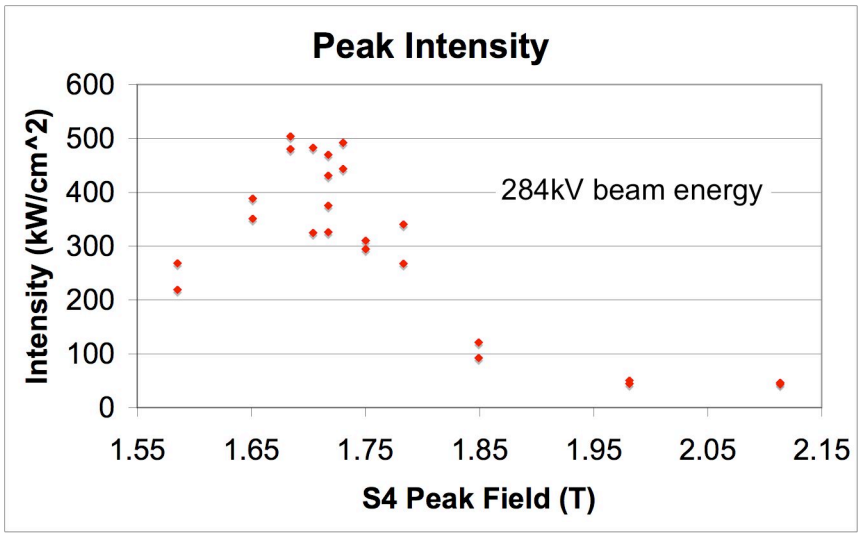

Fig. 8: Parametric scan of beam intensity with final matching solenoid field.

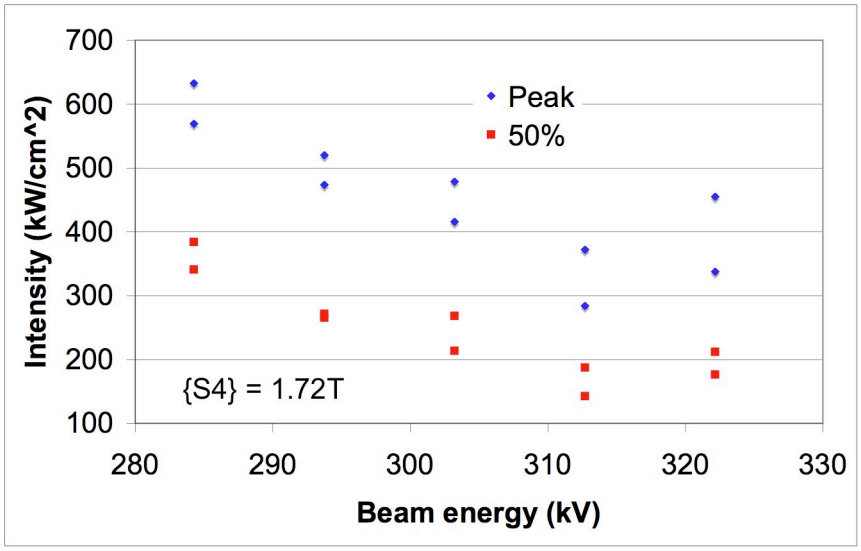

Fig. 9: Parametric scan of beam intensity with beam energy.

Pulse to pulse variations in the beam intensity distribution and centroid position were performed. Fig. 10 shows 3 consecutive, false-color images of beam pulses that display very little variation in the intensity distribution. The jitter in the centroid position is ~100μm. Fig. 11 shows the intensity map of one shot. The full width half maximum for the distribution is ~1mm, with ~100s μm wide peak intensity spot, which is the limit of the CCD camera resolution.

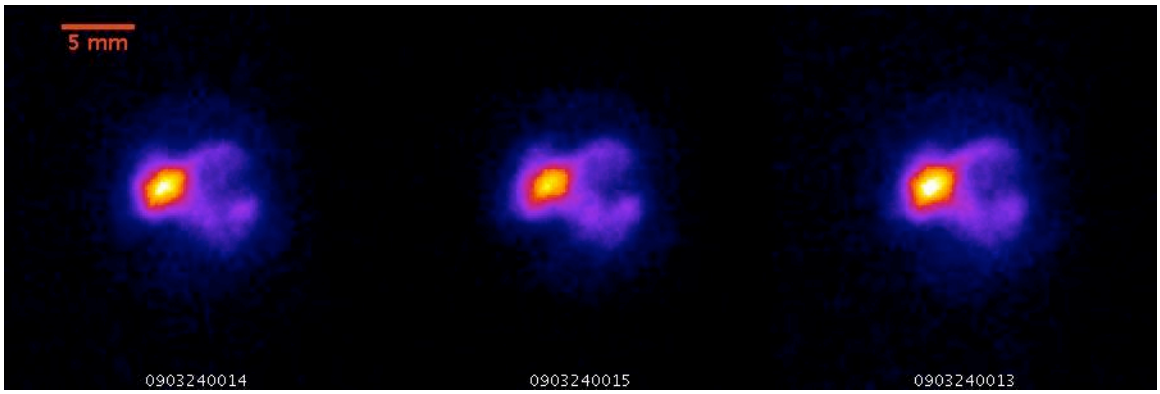

Fig. 10: Montage of beam intensity profiles on target plane scintillator. Three consecutive beam pulses are shown.

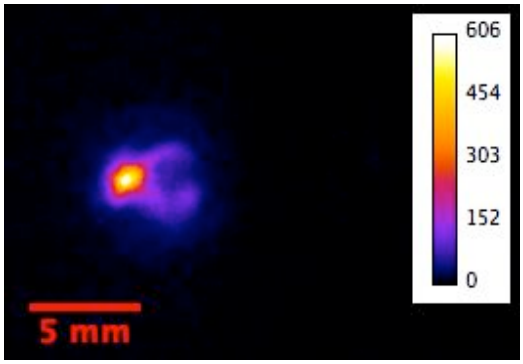

Fig. 11: Intensity map of beam distribution at target plane. Units are kW/cm^2.

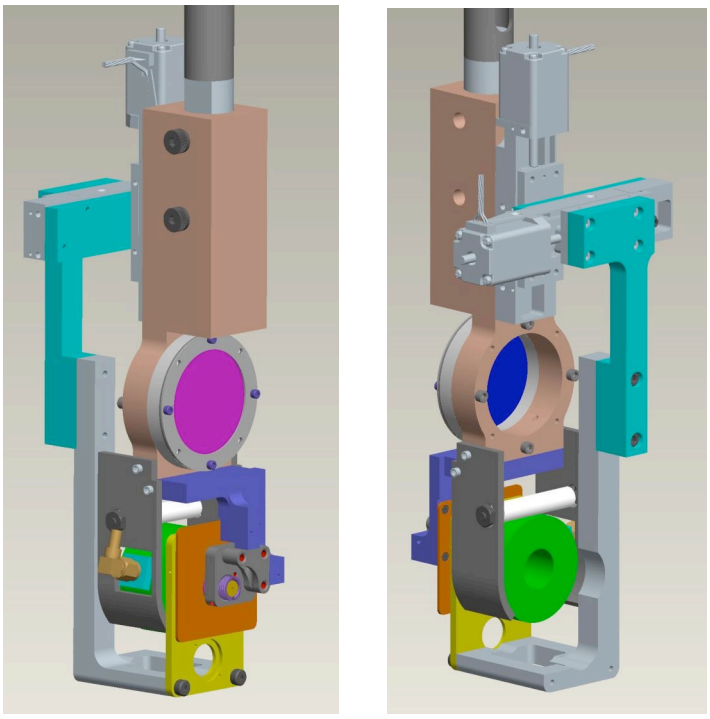
Fig. 12. CAD drawing of new target manipulator. Upstream side (left), downstream side (right).

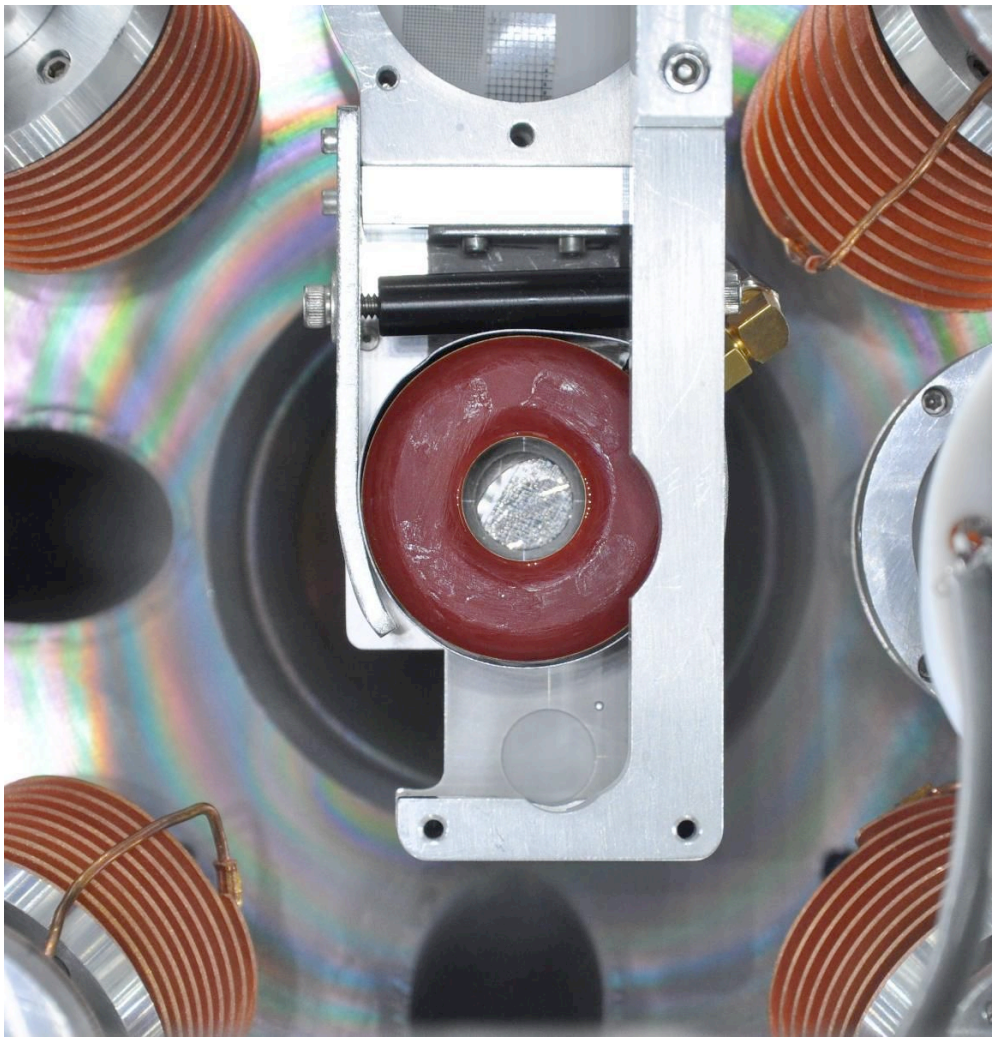

Fig. 13. View from downstream of carbon foil target mounted on the new target positioner in situ in the target chamber. Note the alignment crosshair fiducial marks, and the downstream current transformer (red toroid). The target micro-positioner system allows repositioning the target without moving the pinhole, which is upstream of the target at the center of the crosshairs fiducial marks.

5. TARGET POSITIONER AND DIAGNOSTIC IMPROVEMENTS

The new target holder (Figs. 12-14) has two axes of motor drives to provide two degrees of freedom of remote positioning of the target. These include 2 axes on the target positioner and 2 axes on the light collection optics table (previously there was only 1 axis of motor drive on the light collection optics table). This improvement allows us to remotely position the target and target assembly without breaking vacuum to move the target to an undamaged spot. The target contains a set of improved fiducials and alignment aids for speeding up the process of alignment of the target and light collection optics.

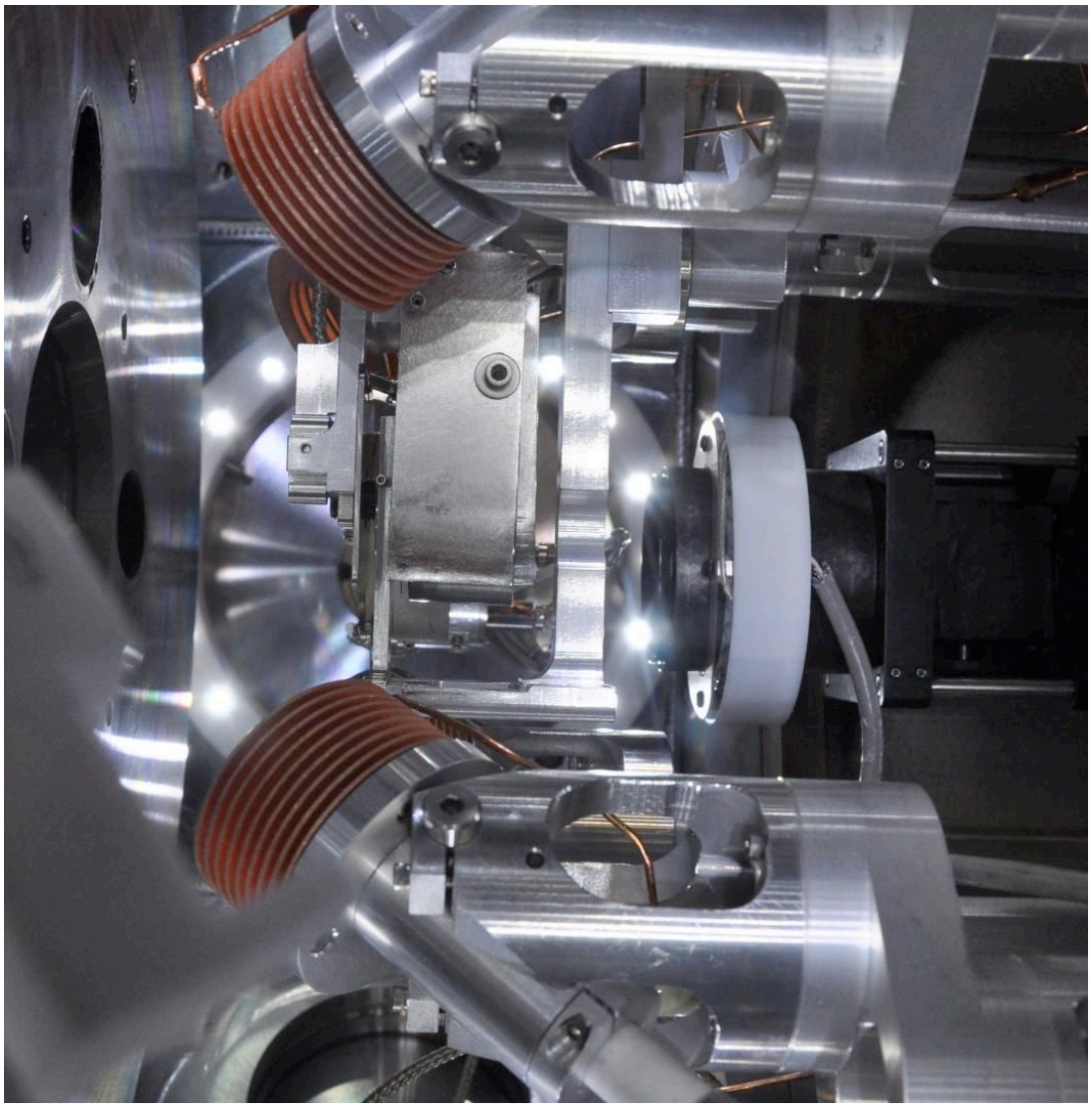

Fig. 14. View into the side port of the target chamber, showing the target positioner, light collection lens of the optical target diagnostic system, and FCAPS plasma injection system.

We have installed a new current monitor downstream of the target. This current monitor is a Bergoz FCT-016-20:1-VAC fast current transformer with a 20:1 turns ratio. The purpose of the current monitor is to measure beam current transmitted through the target as a function of time. For example if a beam current of 30 mA is transmitted through the foil, a signal of 30 mV is expected. In a target thicker than the range of the beam, the beam current transmitted should be negligible even as the target vaporizes since the beam stopping for solid and vapor target material is very similar. This is the case if no droplets form in the target. However we expect to see a change in transmitted beam current if and when the target bunches up into droplets. This diagnostic may therefore be an excellent diagnostic of droplet formation. Initial beam experiments show a beam current signal that is comparable in amplitude to electrical noise coming from the FCAPS plasma

and stray magnetic field from the final focus solenoid. Improved electrical and magnetic shielding are being installed to reduce the interference level.

Image quality and light collection efficiency of the light collection system imaging leg have been improved, by employing a custom f-mount microscope lens near the imaging end of the fiber. This improvement allows for faster beam-target alignment and recording of shorter gated images of the exploding target.

We have also installed an improved video camera to provide a video image of the target during target shots.

Work on further enhancing of pyrometer efficiency is in progress. One possible way to increase light coupling to pyrometer detector is to utilize a 300 μm - 65 μm tapered fiber and a 1-mm diameter ball lens.

An off-line VISAR test showed that it is possible to apply it to the foil targets for measuring target expansion velocity. Previously, it was thought that there is not enough probing-laser reflection from the wrinkled target foil. By utilizing a custom, wide-aperture lens system it was possible to achieve levels of signal sufficient for velocity measurements, however it is marginal. The VISAR will be used in future experiments later in 2009.

We have begun investigation of a new concept for a polarization-based optical pyrometer. It is based on the fact that the polarization of the optical emission from a surface is a function of the angle of emission. The effect may prove to be an excellent passive diagnostic of the emissivity of the surface and of the surface roughness. We may be able to improve the accuracy of the existing pyrometer by providing independent information on the emissivity of the surface. In addition, as the target foil forms droplets, its surface roughness and thus the polarization of the optical emission is expected to rapidly and dramatically change. Further work is planned in this area.

6. EXPERIMENTAL TARGET DATA

Initial beam shots using the new NDCX configuration have been performed using a 400-nm carbon foil target. Fig. 15 shows the carbon target foil after three shots. Because the carbon foil does not adhere well to the nickel support mesh, the foil has a tendency to tear away from the support mesh after a target shot. This is in contrast to the metal foils, which show a well defined hole in the target where the beam heated the target under the pinhole.

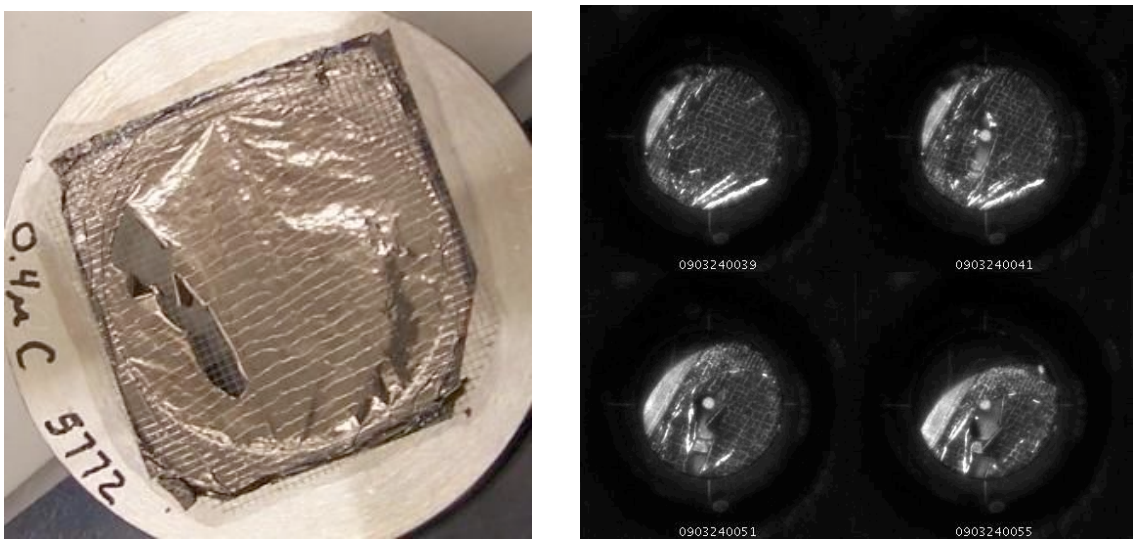

Fig. 15. Carbon foil target after 3 shots. On left, the target foil after removal from the target chamber. On right, images of the foil in situ showing from top left to bottom right the foil before the first shot and immediately after each of the three sequential shots.

Fig. 16 shows a gated camera image of a carbon target foil during a beam heating experiment. The diameter of the pinhole is 1 mm. The image shows that the fireball of hot carbon expands during the first 6 μs from the beam pulse to >2 mm, more than twice the initial diameter of the heated region.

Figs. 17 and 18 show preliminary results from the streak-spectrometer diagnostic. These results indicate a peak target temperature of 4000 K.

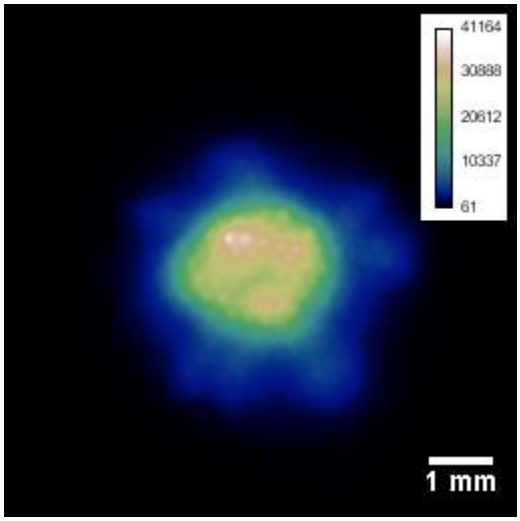

Fig. 16. Gated camera image (gate width = 6 μs) of a carbon target foil heated by a NDCX beam pulse.

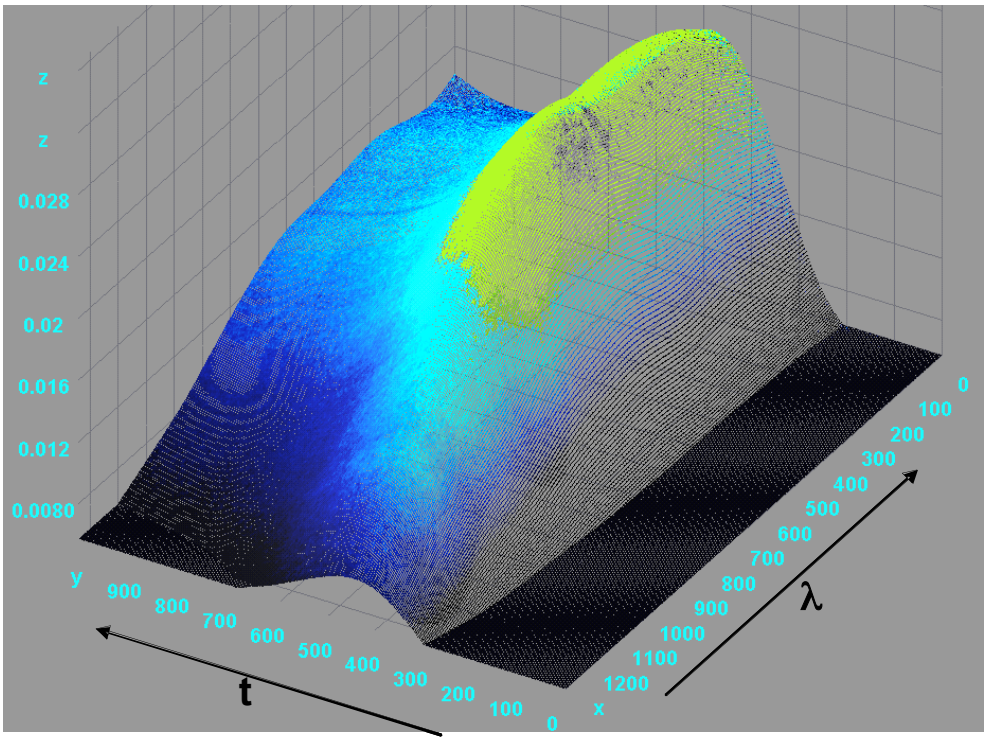

Fig. 17. 3-D plot of absolute spectrum of optical emission from heated carbon target. Time, t, is in units of 10 ns, and wavelength λ is in units of nm.

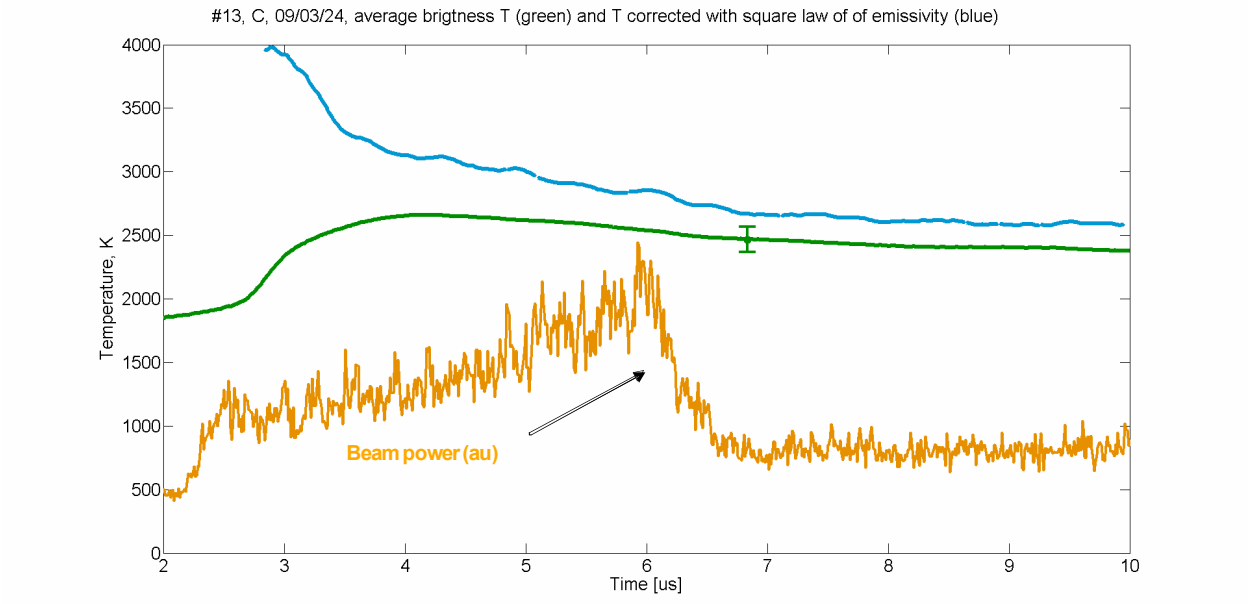

Fig. 18. Results of a preliminary analysis of the streak-spectrometer data from shot #13 (carbon target), showing the brightness temperature, corrected (true) temperature and the optical signal at the streak-spectrometer from beam emission at the target scintillator, which is proportional to the beam power on target.

7. PLANS FOR FUTURE WORK

Future work will involve increasingly sophisticated target experiments using the full set of diagnostics available. Additional tuning of the bunching module waveform will increase the total charge in the highly compressed pulse, and the beam optics will be re-optimized to maximize beam fluence in the compressed portion of the beam pulse.

Planned diagnostic upgrades include those indicated in Section 5, and installation of an aerogel or foil collector for collecting target debris.

8. REFERENCES

1. HIFS-VNL 3rd Quarter 2008 milestone report, June 12, 2008.
2. J.J. Barnard, et al., Accelerator and ion beam tradeoffs for studies of warm dense matter, Proc. 2005 Particle Accelerator Conference, p. 2568
3. P.K. Roy, at al., Neutralized drift compression experiments with a high intensity ion beam, NIM A 577 (2007) 223-230.
4. P.A. Seidl, et al., Plans for longitudinal and transverse neutralized beam compression experiments, and initial results from solenoid transport experiments, NIM A 577 (2007) 215-222.
5. HIFS-VNL 4th Quarter 2008 milestone report, September 16, 2008.